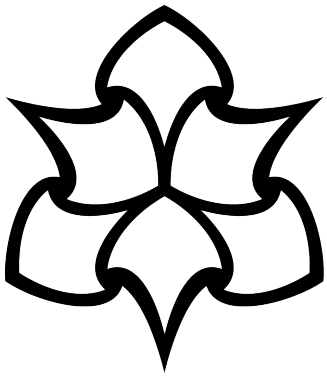

Effect of electropulsing on the fatigue resistance of aluminium alloy 2014-T6

A. Babutskyi[a], M. Mohin[b,]*, A. Chrysanthou[a], Y. Xu[c], A. Lewis[a]

[a]*School of Engineering and Computer Science, University of Hertfordshire, College Lane, Hatfield, Hertfordshire, AL10 9AB, UK*

[b]*School of Science and the Environment, Manchester Metropolitan University, Chester Street, Manchester, M1 5GD, UK*

[c]*School of Aerospace, Transport and Manufacturing, Cranfield University, College Road, Cranfield, Bedfordshire, MK43 0AL, UK*

*Corresponding author.

E-mail address: m.mohin@mmu.ac.uk (M. Mohin)

Declarations of interest: None

Contributions: All authors contributed equally to the research and/or article preparation.

Abstract

The effects of electropulsing on the fatigue resistance of aluminium alloy 2014-T6 were studied in relation to electric current amplitude, pulse duration, and number of repetitions. Utilising the Taguchi method, the present study identified the current amplitude and the duration of the electropulsing as the two critical treatment parameters for improved fatigue resistance. A 97% fatigue life improvement was achieved under the electropulsing conditions that were applied. An increase in microhardness and a decrease in electrical conductivity due to electropulsing were correlated with enhanced fatigue resistance in the alloy. Mechanisms related to the effects of the electropulsing treatment were elucidated based on observations from scanning electron microscopy (SEM) and transmission electron microscopy (TEM) as well as numerical simulation results. The mechanisms identified by observation included dislocation movement and the secondary precipitation of GP-zones. Further explication of these mechanisms was provided by the application of a “magnetic field’’ model.

Keywords: Electropulsing, Aluminium alloy, Fatigue, Dislocations, Precipitation hardening, Fracture.

1. Introduction

Fatigue is the progressive and localised material degradation of a component caused by repeatedly applied loads. Fatigue is dependent on multiple factors [1, 2], including stress concentration, fabrication, heat, and surface treatments and finishing. Improvements in the fatigue resistance of metallic components can be achieved by careful design, detailing, fabrication, and alloying [3, 4]. In addition, various types of thermo-mechanical processing [5, 6] and other techniques including surface treatments to induce compressive residual stresses [7, 8] are being used. The development of new cost-effective techniques for fatigue resistance enhancement of metals is a challenge that is being addressed by both academic and industrial researchers. Among these techniques, the application of electropulsing [9-20] and the application of magnetic fields [21-23] are attracting attention, yet systematic investigations are still lacking. The similarity between these two treatments must be noted as a changing electric current in a conductive medium produces a magnetic field and vice versa. Therefore, during treatment, an electrically conductive material is subjected to an electric

current and a magnetic field simultaneously. Application of a permanent magnetic field to enhance the fatigue resistance of metals has also been a subject of interest [23].

Previous investigations have reported that electropulsing can extend the fatigue life of steel [10, 14, 16, 19, 20, 24], copper [25], titanium [9, 13] and aluminium [26, 27] alloys. Levitin *et al.* [9] examined the effects of electropulsing on the fatigue resistance of titanium and found that fatigue life increased by 25-50%. Electropulsing was observed to lead to the reduction in residual stress and homogenisation of the microstructure as well as stress relaxation. Sosnin *et al.* [15, 16] reported a 54-76% improvement in the fatigue life of austenitic steels as a result of electropulsing and proposed stress relaxation as the mechanism of enhancing the fatigue resistance induced by this treatment. Tang *et al.* [10] examined the effects of electropulsing on the repair of fatigue damage of notched stainless steel (SUS31) plate with focus on the crack initiation resistance at the notched area by using a tensile-tensile fatigue test. The study showed that crack initiation resistance improved by 26%. The authors reported that the high-density electric current was able to restore microhardness to a nominal level to enhance fatigue resistance. In another study [11], the same group of researchers varied only the pre-fatigue level to investigate how effective electropulsing was in restoring fatigue life. The pre-fatigue level was defined as the percentage of the number of fatigue cycles applied to untreated samples prior to the fatigue initiation life. The researchers described the number of cycles required for the crack to grow up to 25μm as the crack initiation life. The study showed that electropulsing at 43% and 85% of fatigue crack initiation life increased the fatigue crack initiation life by 6% and 21%, respectively. Thus, the effect of electropulsing was more prominent during the later stages of the crack initiation process when sufficient fatigue damage had accumulated. In other research, Konovalov *et al.* [12] reported that electropulsing enhanced the fatigue life of stainless steel (0.45C17Mn3Al) by 72%, while Zhao *et al.* [14] demonstrated an improvement in the thermal fatigue life of cast-hot work die (CHWD) steel. An improvement of 140% in the fatigue crack initiation life was observed in the latter study.

Based on evidence from the literature, electropulsing can enhance the fatigue life of many metals and alloys. However, full exploitation of the technique is unlikely to occur until systematic research is able to fully elucidate the mechanisms that lead to improved fatigue resistance and to identify which electropulsing treatment parameters are most strongly correlated to fatigue life enhancement. The aim of this paper is to address the knowledge gap by utilising a systematic experimental investigation to understand the effect of electropulsing on the fatigue resistance of aluminium alloy 2014-T6. As such, the electropulsing intensity, measured as electric current density, pulse time and number of repetitions during the treatment were investigated using the Taguchi approach [28] which deals with process optimisation and determines the most effective parameters for testing and processing [29] to yield the best possible fatigue life enhancement.

2. Material and experimental procedures

2.1. Material, samples and test techniques

The chemical composition of aluminium alloy 2014-T6 is shown in Table 1.

Table 1 The chemical composition of aluminium alloy 2014-T6 [30].

Element	Al	Si	Fe	Cu	Mn	Mg	Cr	Zn	Ti	Others
Weight (%)	Balance	0.5-1.2	0.7	3.9-5.0	0.4-1.2	0.2-0.8	0.1	0.25	0.15	0.15

Samples for testing were machined using an XYX Proturn SLX1630 CNC lathe. The geometrical details of the round hourglass fatigue test samples are shown in Figure 1. Samples for conductivity

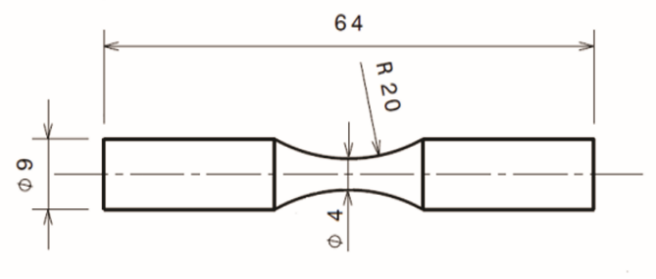

Figure 1. Geometrical details of the fatigue test sample (dimensions are in mm).

tests were machined, as shown in Figure 2a. Samples for microhardness tests were cut from the same samples (Figure 2b). All the samples were machined from 12.7mm diameter extruded bars

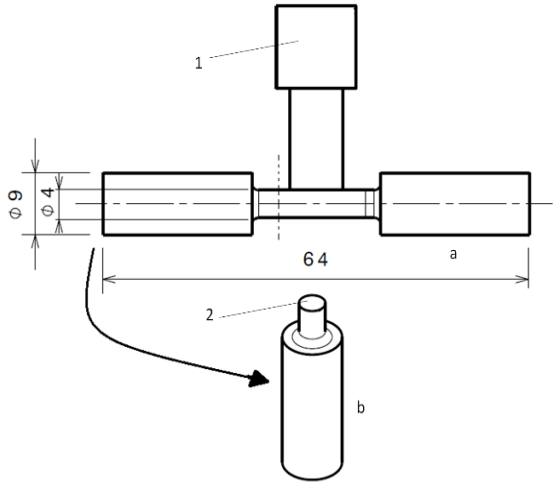

Figure 2. Sample for conductivity (a) and microhardness (b) tests. 1 – conductivity probe; 2 - surface for microhardness measurements (dimensions are in mm).

from the same batch and subsequently underwent fine turning to reduce adverse effects from scratches. A Motopol 2000 grinder/polisher was used for gradual grinding and polishing of the samples for microhardness testing.

A single-end, rotating cantilever test machine (SM1090) with a dead load was used during fatigue tests at a rotating bending frequency of 60Hz and a load ratio, *R* of -1. Results for untreated samples are presented in Figure 3. The Engineering Sciences Data Unit (ESDU) database [31] provided fatigue life data for aluminium alloy 2014-T6 samples of a similar size (i.e., minimum neck depth of

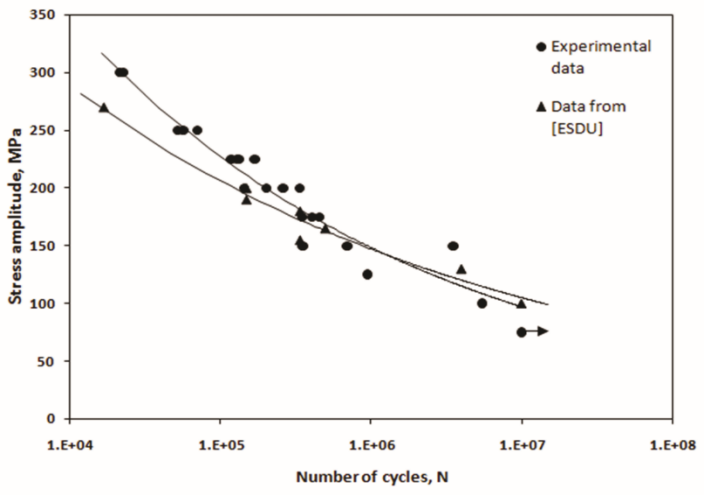

Figure 3. Stress vs number of cycles (S-N) curves of aluminium alloy 2014-T6.

6.4mm), as plotted in Figure 3. These results provided the baseline fatigue data to assess the effect of electropulsing on the fatigue resistance of aluminium alloy 2014-T6. Electrical conductivity measurements were conducted using a SIGMATEST 2.069. Measurements were taken at four equidistant points on the outer circumference of the 4mm diameter samples. The conductivity was measured five times at each point, and the average value was used to analyse the effect of electropulsing on the conductivity of the alloy. The microhardness was measured using a semiautomatic DuraScan 20 microhardness tester.

A JEOL JSM-5700F scanning electron microscope (SEM), was utilised to examine the fracture surfaces of the samples after fatigue testing. Then, transmission electron microscopy (TEM) was conducted utilising an FEI/Philips CM-20 to provide a detailed characterisation of microstructural changes in the alloy as a result of the electropulsing treatment.

2.2. Treatment by electropulsing

A pulsed electric current generator (Figure 4) was used for the electropulsing treatment. The equipment included a high-voltage supply (5kV), a capacitor (100μF), variable inductance, a ballast

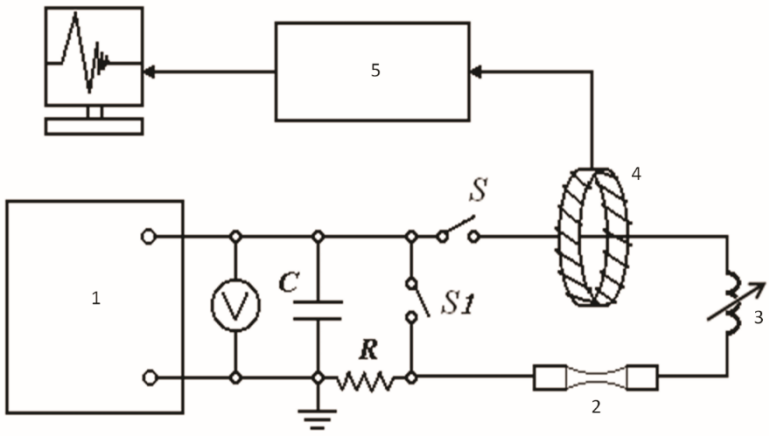

Figure 4. Treatment diagram: 1 – high voltage supplier, 2 – sample, 3 – variable inductor, 4 – Rogowski coil, 5 – analogue-to-digital converter, *C* - capacitor, *S* and *S*1 – switches, *R* – ballast resistor.

resistor and switches. During the electropulsing treatment, a sample was connected to the generator (Figure 4) and treatment was fulfilled by discharging the capacitor that had been charged to a voltage of 0.15–5kV. The pulsed electric current flowing into the circuit during the discharge was in the form of a decaying alternating current and was registered using a calibrated Rogowski coil. A high-speed analogue-to-digital converter (PicoScope 4424) was employed to register the profile of the discharged current. Following treatment, the samples were stored at room temperature for 24 hours prior to testing.

The Taguchi method [28] was used in the design of the experiments (DoE) to determine the parameters that would ensure maximum processing effects within the ranges of their variation. While the reliability of the test data could be improved by increasing the number of test samples, the Taguchi method optimised the test matrix by using an orthogonal array to reach an optimum result with a minimum number of tests at minimum cost. Several research papers describe how this approach was used previously to optimise the relevant parameters for fatigue performance [29, 32-34]. In the present study, Minitab 17.0, a commercially available statistical software package that enables DoE [35] was utilised to implement the Taguchi method.

Three parameters or factors were considered for electropulsing treatment. These were the electric current amplitude (A), the current pulse duration (B) and the number of repetitions during treatment (C). The corresponding values are shown in Table 2.

Table 2 Electropulsing treatment parameters.

Level		Parameters		
		A	B	C
		Current, kA	Pulse duration, s	No. of repetitions
Low	1	0.73	0.00008	1
Medium	2	1.0	0.03	2
High	3	1.2	0.1	4

Three levels of treatment for each parameter were used including low (1), medium (2) and high (3). The current amplitude and its duration were varied by changing the voltage for charge and inductance. Due to natural restrictions caused by the generator design, voltage, capacitance and inductance, the maximum discharge current was about 1.2kA, and the maximum and minimum current durations were 0.1s and 0.00008s, respectively. According to the Taguchi DoE, nine sets of experiments or treatment parameter combinations ($L_9 = 3^2$ orthogonal array) were designed as shown in Table 3 in the results section.

Temperature registration during the treatment was undertaken using a K-type thermocouple with 0.2mm diameter wires and a PicoLog 6 data logger. The thermal effect of the treatment was judged to be insignificant as the application of a 1.2kA electric current pulse with 0.1s duration caused an increase in the sample temperature of only approximately 2^{o}C.

3. Results

3.1. Fatigue tests

In total, six untreated samples were fatigue tested at the same stress amplitude of 200MPa and their average fatigue life was 239095 cycles. During the implementation of the Taguchi DoE, three samples for each electropulsing treatment parameter combination were treated and fatigue-tested at the same level of stress amplitude of 200MPa. Later, for Taguchi experiment No. ix, three additional samples were treated and subsequently fatigue-tested. The results are presented in Table 3.

Table 3 Taguchi DoE $L_9 = 3^2$ orthogonal array, corresponding experimental fatigue life, average fatigue life and signal to noise ratio (S/N).

Exp. number	Factors			Fatigue life, cycles	Average fatigue life, cycles	Signal to noise ratio (S/N)
	A	B	C			
i	1	1	1	223245, 260457, 239297	241000	107.6
ii	1	2	2	223873, 298425, 309542	277280	108.9
iii	1	3	3	322360, 401833, 326485	350226	110.9
iv	2	1	2	309125, 249134, 229782	262680	108.4
v	2	2	3	323484, 253510, 393686	323560	110.2
vi	2	3	1	384143, 360730, 312150	352341	110.9
vii	3	1	3	293321, 248464, 229728	257171	108.2
viii	3	2	1	300648, 323873, 262207	295576	109.4
ix	3	3	2	460932, 457860, 448647, 516247, 350492, 597328	471919	113.5

In the Taguchi method, the variation (deviation) between the experimental and desired results is converted into a signal to noise ratio (S/N) value [29]. The (S/N) value can be derived based on one of three different scenarios: the nominal-the-best situation, the bigger-the-better situation and the smaller-the-better situation. To determine the optimal effect of electropulsing on the fatigue resistance of 2014-T6, the bigger-the-better situation was utilised as a longer fatigue life was desirable. The (S/N) ratios illustrated in Table 3 were calculated based on the bigger-the-better scenario which is defined by the equation:

$$S/N = -10\log\left[\sum_{i=1}^{n}\left(1/y_i^2\right)/n\right] \quad (1)$$

where n is the repeat number, and y_i is the measured variable value (fatigue life cycles).

The (S/N) ratio can characterise the effect of the input of an experiment. To achieve a longer fatigue life, this ratio needs to be maximised. The main effects plot for the (S/N) ratio is shown in Figure 5, which demonstrates that the (S/N) ratio increased at each level above the initial level of 1 in the case

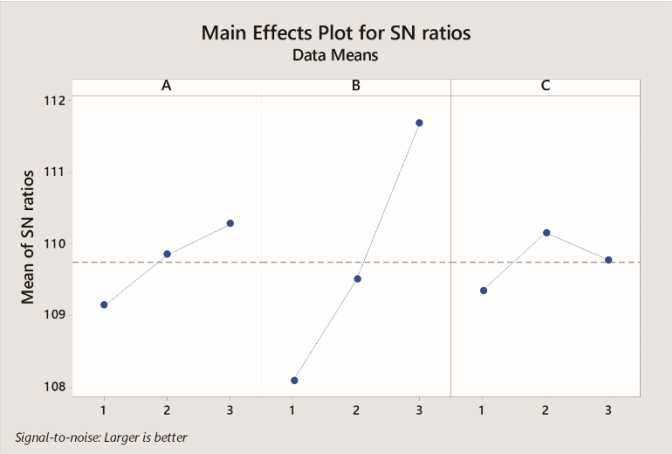

Figure 5. Main effects plot for the signal to noise ratio (S/N).

of factors A and B. However, this (S/N) ratio pattern was not reproduced for factor C. For factor C, the (S/N) ratio increased from level 1 to level 2 as it had done in the case of each of the previous two factors, but then declined for level 3. While the (S/N) ratio for level 3 in the case of factor C remained higher than the value for level 1, it demonstrated a decrease from the (S/N) value achieved at level 2. It must be noted that at level 3, the increase of (S/N) ratio for factors A and B is big enough to cancel out the decrease of (S/N) ratio for factor C at level 3. Therefore, the beneficial effect of electropulsing increased with simultaneous increases in the pulsed current amplitude, the pulse duration and the number of repetitions. However, the beneficial effect of electropulsing started to decline when the number of repetitions reached 4, as demonstrated in the case of level 3 and its impact on factor C. Thus, the array 3 – 3 – 2 of A – B – C factors (i.e., Taguchi experiment No. ix) appeared to provide the optimum combination of factors or parameters among the combinations tested. The average fatigue life of the samples treated under the conditions pertaining to the optimum parameters was 471919 cycles, which provided a fatigue life enhancement of 97% compared to the original, untreated condition. The overall percentage increases in fatigue life obtained under various combinations of treatment parameters are presented in Figure 6.

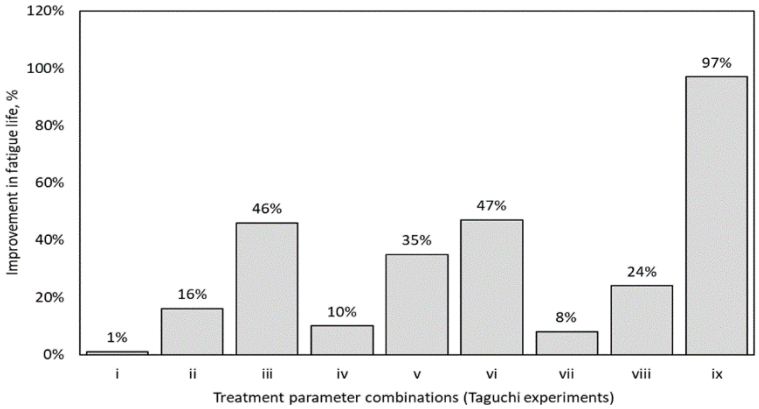

Figure 6. Fatigue life improvement depending on treatment parameter combinations.

3.2. Microhardness and conductivity

The electropulsing treatment, as applied in Taguchi experiment No. ix was used to investigate its effect on microhardness, as illustrated in Figure 7. Measurements were taken at a range of points

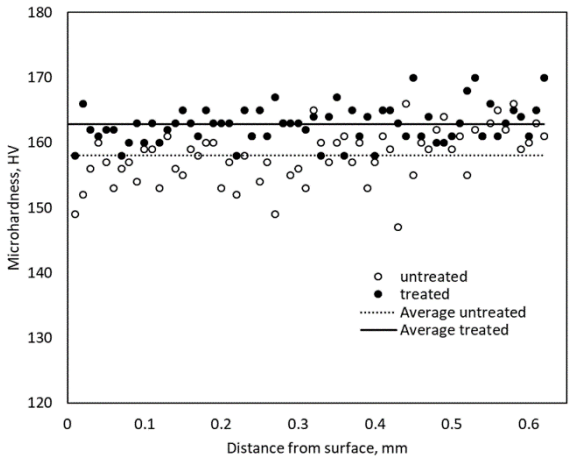

Figure 7. Effect of electropulsing treatment on microhardness.

from the outer edge of the samples to nearly the centre of the test samples at their minimum cross-section (i.e., 4mm diameter). The microhardness of the treated samples was higher compared to that of the untreated samples. The average measured value and standard deviation of the microhardness of the untreated alloy were 158HV and 4.16HV, respectively, whereas the average value and standard deviation of the microhardness of the treated alloy were 163HV and 2.88HV, respectively. Therefore, the increase in microhardness due to electropulsing was approximately 3%. Additionally, the value of the coefficient of variation of hardness for each of the treated and untreated alloys was 1.78% and 2.63% respectively which suggested that the homogeneity of the treated sample had increased.

The Taguchi experiment No. ix parameters were also applied to the samples used for the conductivity test. Based on 20 measurements for each treated and untreated sample, it was concluded that the overall electrical conductivity of the treated samples decreased by 1.2%. The observed increase in the microhardness and decrease in the electrical conductivity as a result of electropulsing were indicative of precipitation hardening of the alloy.

3.3. Microstructure

The features of the final fracture surfaces of the treated and untreated samples from Taguchi experiment No. ix were examined using SEM (Figure 8). The corresponding fatigue life of the treated

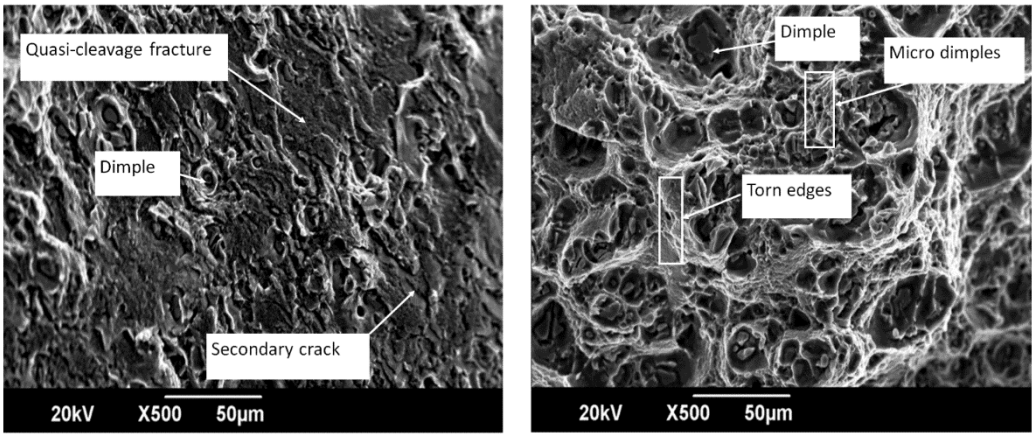

Figure 8. Final fracture surfaces: (a) untreated and (b) treated samples.

and untreated samples at a stress amplitude of 200MPa were 516247 and 2666446 cycles, respectively. In the present study, both samples exhibited a mixture of dimple and cleavage fractures at the surface of the final fracture. However, the untreated sample (Figure 8a) exhibited more quasi-cleavage fracturing [36] in the fracture surface under examination, while the treated sample contained more ductile dimple features of diverse sizes (Figure 8b) similar to those discussed in [37, 38] at the fracture surface. A few quasi-cleavage fractures were still exhibited by the treated sample; however, overall, the fracture surface consisted of ductile features such as torn edges [39], peaks [40] and ductile dimple features which can be categorised as large equiaxed dimples and micro-dimples (Figure 8b). The fracture surface of the untreated sample also exhibited secondary cracks similar to those observed in [41]; however, such cracks were not visible in the treated sample.

The Taguchi experiment No. ix parameters were also used when treating the material for the TEM study. Figure 9a shows evidence of dislocation pile-ups in the untreated sample. By contrast, Figure 9b shows that the treated sample exhibited fewer dislocation pile-ups and more uniform dislocation

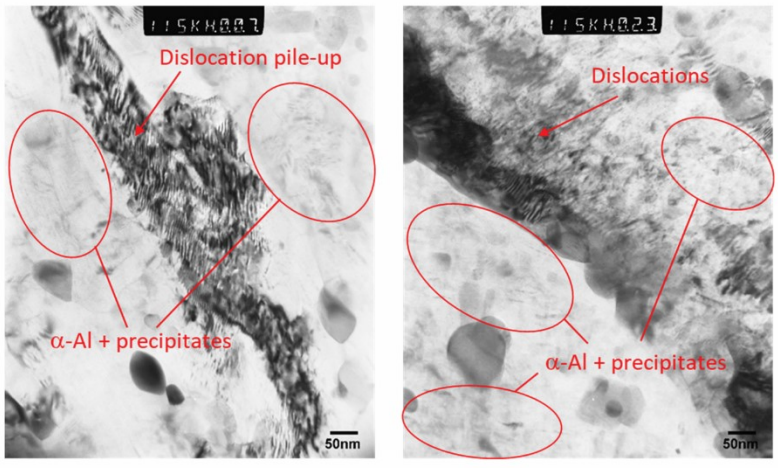

Figure 9. TEM images taken from the near-surface area of 4mm diameter specimen: (a) untreated and (b) treated.

distribution. In addition, individual pile-ups were much smaller in size and less dense. Figure 9 also presents evidence that the precipitation of GP-zones was more pronounced in the treated sample compared to the untreated one. These precipitates were also more uniformly distributed within the treated alloy compared to the untreated example.

4. Discussion

4.1. Distributions of electric current and magnetic field during the treatment

The results in Figures 5 and 6 illustrated that the amplitude of the pulsed electric current and the pulse duration were the main parameters affecting the fatigue resistance of the treated samples. It must be noted that during electropulsing, the samples also experienced a pulsed magnetic field as an integral side-effect of the current passing through the current-carrying sample. The magnitude of this field within the current-carrying sample was a function of the current (I) passing through the sample and the radial distance (r) across the central axis of the sample according to

$$B = \mu_0 lr/(2\pi R^2) \quad (2)$$

where μ_0 is a constant (i.e., the vacuum permeability) and R is the sample radius. Therefore, the magnetic field inside the sample was distributed proportional to r and varied with the current.

Numerical modelling based on finite element (FE) analysis utilising QuickField 6 software was employed to estimate the magnitude of treatment parameters (i.e., current, magnetic field distribution, and heating effect). The simulation was conducted in two steps; the first step was a solution of the transient electromagnetic field sub-problem, while the second was a solution of the sub-problem of transient heating caused by Joule loss. The sub-problems were solved for 2-D formulations applicable to a circular rod of 4mm diameter. The simulations were performed using the following physical properties of the aluminium alloy: density, ρ = 2800 kg/m^3; electrical conductivity, σ = 22.53x10^6 S/m; thermal conductivity, λ = 154 W/(m·K); and specific heat, c = 880 J/(kg·K). All the properties in the simulations were assumed to be independent of temperature. Since the magnetic field strength during processing was high, the relative permeability was taken equal to μ = 1. Also, as the duration of the treatment was short, heat exchange with the ambient air was not considered. Zero initial conditions were assigned. The variation of the current passing through a circular rod was in the form of a decaying sinusoid

$$I(t) = I_0\, exp(-a \cdot t)\, sin(2\pi t/t_{PEC}) \quad (3)$$

where t_{PEC} is the period of current oscillation determined from the recorded profiles of the pulsed electric current. The values of I_0 were also determined based on best fitting to the electric current data points. Examples of the full current data points utilised during numerical modelling are presented in Figure 10.

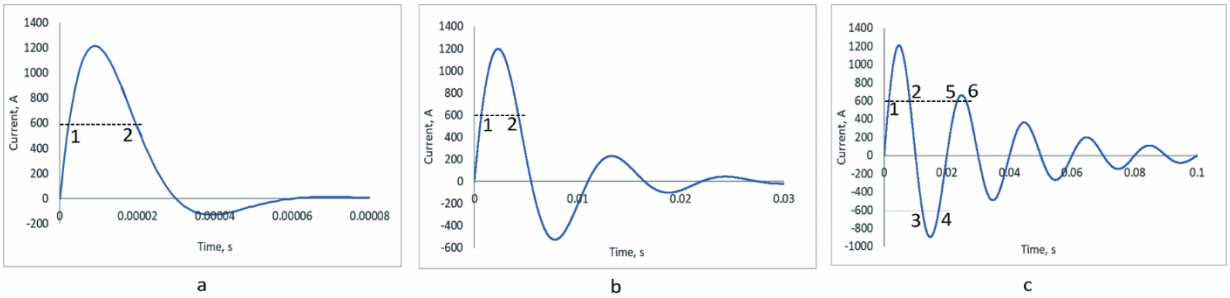

Figure 10. Electric current variations from modelling of the treatments using a current amplitude of 1.2kA and pulse durations 0.00008s (a), 0.03s (b) and 0.1s (c).

The results of the numerical modelling are presented in Figure 11. The figure illustrates the distribution of the electric current and the magnetic field flux density in cross-section and the

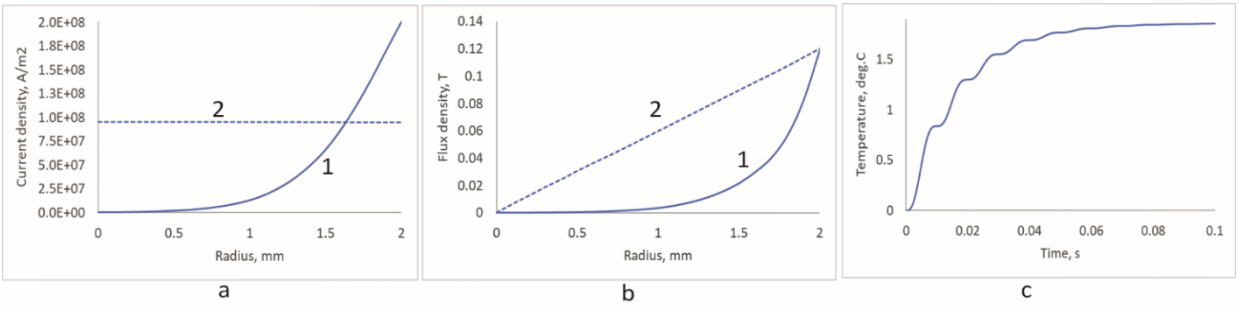

Figure 11. Distributions of electric current (a) and magnetic field flux density (b) in cross-section during treatments for current amplitude of 1.2kA and pulse durations of 0.00008s (1) and 0.1s (2), and temperature rise due to application of one pulse with current amplitude of 1.2kA and pulse duration of 0.1s (c).

temperature increase (up to 1.85°C) due to the treatment. The data for an electric current pulse duration of 0.03s are not presented because they are identical to the data for the pulse duration of 0.1s. The distribution corresponds to the moment when the highest level of the full electrical current (i.e., 1.2kA) passes through the sample (see Figure 10). The results demonstrate the presence of a significant ‘‘skin effect’’ [42] in the case of a pulse duration of 0.00008s. In the case of pulse durations of 0.03s and 0.1s, the entire cross-section is affected by the pulsed electric current of the same density. At the same time, the magnetic field intensity increases linearly with the radius and affects a much bigger part of the cross-section in comparison with the 0.00008s pulse duration.

4.2. Effect of electric current and magnetic field on dislocations rearrangement and precipitation

The effect achieved by the treatment cannot be associated with the heat effect as the registration and numerical modelling show a negligible temperature rise of about 2°C which cannot promote any changes in the metal. The possible origin of the changes is via the non-thermal effect of the electric current and magnetic field as previously discussed in the literature [9-23, 43]. Based on TEM observations as well as on measurements of microhardness and conductivity, it can be concluded that the treatment causes increased precipitation of GP-zones and leads to rearrangement of dislocations (see Figure 9).

The high-density electropulsing can lead to dislocation motion due to the electron wind force [44, 45]. This effect of the pulsed electric current on the crystal lattice of a metal can be evaluated. The basic relationships determining the kinetics of the interaction between the conduction electrons and the crystal lattice in accordance with the existing understanding of the electrical conductivity mechanism [46] allow the estimation of the current density, electric field intensity, and electrical resistivity utilising the equations below:

$$\begin{aligned} i &= evn_0; \\ \frac{dU}{dx} &= E = \rho i; \\ \rho &= 2m_e/(n_0 e^2 t_0) \end{aligned} \tag{4}$$

where i is the current density (A/m^2), e is the electron elementary charge, v is the velocity of electron drift (m/s), n_0 is the number of conduction electrons per unit volume (1/m^3), U is the electric potential (V), E is the electric field intensity (V/m), ρ is the electrical resistivity (Ω·m), m_e is the electron rest mass equal to 9.10956·10^{-31}kg and t_0 is the mean free time of an electron between ionic collisions.

From these equations (4), the kinetic energy of the electron drift by the action of the electric field under an isotropic scattering of electrons can be derived [47] as

$$K_e = m_e v^2/2 = eE \cdot (vt_0) = \rho i(evn_0)t_0/n_0 = \rho i^2 t_0/n_0 \tag{5}$$

At fixed current density and electrical resistivity, electrons ↔ crystal lattice interaction parameters can be determined by Equations (4) and (5). The increase in the kinetic energy of an electron within its free path for aluminium, as calculated by Equation 5 at a current density of 0.1kA/mm^2 is ΔK_e ≅4.9x10^{-17}eV/atom, a value which is significantly less than the change in the kinetic energy due to thermally induced atomic motion, ΔK_T, at an increase in temperature, T, by 1°C:

$$\Delta K_T \cong kT \cong 8.61\text{x}10^{-5}\text{eV} \tag{6}$$

where k= 8.617333262145×10^{-5} eV·K^{-1} is the Boltzmann constant.

Thus, in a perfect crystal lattice, a single interaction between an electron and an atom does not exert significant influence on the motion of a metal atom. This increase in the interaction energy is negligible, even if the main type of interaction is the predominant interaction between the flowing electrons and atoms in the vicinity of dislocations. In this case, the ratio of the total density of atoms, n, to the density of dislocations, n_d, is $n/n_d \approx 1.2\text{x}10^5$ which corresponds to a density of dislocations of 10^{10}/cm^2. From this, an effective increase in the kinetic energy of all “defective” atoms can be estimated as ΔK_{ef} ≅5.6 x10^{-12}eV/atom. Again, this value is still negligible in terms of thermal atomic motion, see equation (6). Therefore, a mechanism based on dislocation movement involving the direct interaction of flowing conduction electrons and dislocations for current densities of up to 0.2kA/mm^2 can be excluded.

A uniform pattern of dislocations similar to that presented in Figure 9 has also been observed for steel and titanium as a result of magnetic field treatment in earlier research [47, 48]. Ma *et al.* [49] reported an increase in the number of dislocations in steel as a result of magnetic treatment; this

was attributed to a “magneto-stress” which acted on the dislocations and activated Frank–Read sources and dislocation slip increasing the dislocation density. However, the aluminium alloy 2014-T6 is paramagnetic and its magnetisation is negligible in comparison with steel. Therefore, this mechanism cannot be used to explain the observations of the present research. A more likely model that can be used to explain the changes caused by the magnetic field in paramagnetic materials was presented by Molotskii [50-53]. It is suggested that the application of the magnetic field can change the spin multiplicity of the radical pairs formed by dangling bonds of dislocation cores and paramagnetic obstacles. This change is more likely to induce depinning of dislocations.

According to these studies [50-53], only in the ground singlet (S) state where the electron spins are antiparallel, a strong bond between atoms exists. In the case of parallel spins arising in the presence of a magnetic field (i.e., in the case of triplet (T) state), the bond is weak or even absent. The S-to-T transition becomes possible and the population of T states in dislocation-obstacle systems increases and enables dislocation depinning under the application of a magnetic field. The depinning and subsequent movement and rearrangement of dislocations can take place if there is a source of potential energy to support the process as the S-to-T transition only has a triggering effect. The available potential energy is the energy stored in a plastically deformed material as a result of previous metal-working processes such as rolling, drawing, extrusion, etc. The stored energy can be significant and it has been shown to reach more than 60% of the input plastic work at low levels of plastic strain for alloys such as aluminium alloy 2024-T3 in the study of Ravichandran *et al.* [54].

As the aluminium alloy 2014-T6 bars used during sample manufacturing were obtained by extrusion, the presence of stored energy associated with the residual stresses in the material was very likely. The secondary cracks in the untreated metal (Figure 8a) could have been the result of the existence of these residual stresses. Having become free following depinning, the dislocations could travel due to the effect of the available stored energy (residual stresses) in the processed metal. As a result, piled-up dislocations could become evenly redistributed (Figure 9b). This model could explain not only the movement of dislocations after depinning but also the increase in the density of precipitates illustrated in Figure 8b, as confirmed by the decrease of the electrical conductivity of the alloy after the electropulsing treatment [55-57].

The aluminium alloy 2014 used in the present study was supplied in the T6 temper which meant it had been solution heat-treated and artificially aged. It was clear that some level of residual or “free” solute Cu remained in solid solution in the alloy. Thus, it may be speculated that the application of the magnetic field increases the population of T states in systems composed of Al and “free” solute Cu atoms. As a result of the action of the magnetic field on the aluminium alloy 2014-T6, increased diffusion mobility of Cu atoms takes place causing secondary ageing which is accompanied by an enhancement in strength and fracture toughness [58]. This secondary precipitation and decrease in the tensile residual stresses may be the reason for the increase in the observed hardness [59] and

for the significant reduction in the scatter of the hardness values for the treated metal indicating homogenisation of its structure.

It is reasonable to expect that as the magnetic flux increases, an increase in the population of T states also takes place. The duration of the treatment also has an effect on the material, as dislocation reordering and GP-zone precipitation are time-dependent events. It is possible to estimate the duration of the treatment in the case of pulsed electric current profiles presented in Figure 10; at currents higher than 600A for Taguchi experiments vii, viii and ix (with the highest current), the shortest pulse (experiment vii, Figure 10a) is equal to t_2-t_1 ≈ 18μs. For the medium duration pulse (experiment viii, Figure 10b), it is equal to t_2-t_1 ≈ 3.6ms and for the longest pulse (experiment ix, Figure 10c), it is equal to (t_2-t_1) + (t_4-t_3) + (t_6-t_5) ≈ 14ms. It is evident that treatment efficiency increased with an increase in treatment duration, as shown in Figure 12.

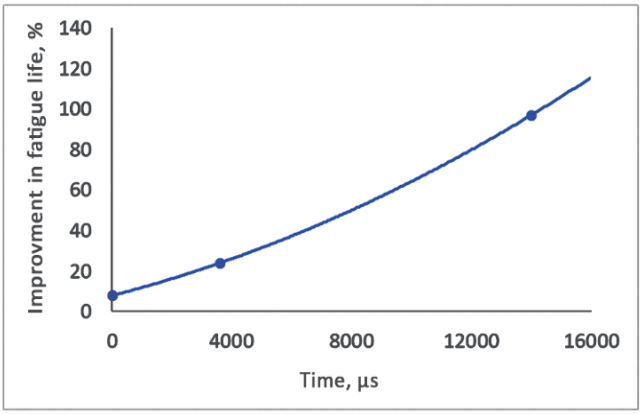

Figure 12. Dependence of the improvement of fatigue life on exposure time at an electric current higher than 600A for Taguchi experiments vii, viii and ix.

It must be noted that the parameters of treatment (i.e., electric current/magnetic flux densities and pulse durations) used in this research were limited by the equipment that was utilised. However, the parameters utilised are not uncommon, and there are many other options available that generate higher magnetic field flux densities (i.e., higher than 0.12T) for much longer duration as used in a recent study [60]. Electropulsing is by its nature both a current inducing and a magnetic field inducing treatment for metals. The effects of the magnetic field induced appear to be complex and a likely reason as to why the understanding of all the effects of electropulsing is still a challenge for researchers. More research in solid-state and fundamental physics to further understand the effects of electropulsing to determine optimal treatment parameters is required. In this study, a “magnetic field” model was used to explicate the results, but the possible effect of conduction electrons on dislocations (i.e., “electron wind” model) during treatment should not be excluded completely.

5. Conclusions

This experimental study demonstrated that the application of electropulsing at a high current density can improve the fatigue resistance of aluminium alloy 2014-T6. The Taguchi approach identified the

current amplitude and the duration of the electropulsing as the two critical treatment parameters for improved fatigue resistance. The number of repetitions of the treatment was found to be much less significant than the first two parameters. Electropulsing was observed to cause movement of dislocations as well as secondary precipitation that led to an increase in microhardness and a decrease in conductivity. There was a negligible increase in temperature of about 2°C as observed by both measurement and numerical modelling and it was concluded that the effects of the electropulsing were achieved non-thermally. The magnetic field induced by the application of the electropulsing triggered dislocation movement that was supported by the energy stored in the plastically deformed material and acted as a driving force for dislocation rearrangement. In addition, secondary precipitation, homogenisation of the microstructure and enhanced ductile fractographic features were observed in samples after the electropulsing treatment. These effects resulted in an increase of up to 97% in the fatigue life of the investigated alloy. 5

Acknowledgement

This research was supported by the Marie Curie International Incoming Fellowship scheme within the 7th European Community Framework Programme Grant number PIIF-GA-2010-274324.

Data statement

The data used in this manuscript is available for reproduction upon request.

References

[1] B. Boardman, Fatigue resistance of steels, ASM International, Metals Handbook. Tenth Edition 1 (1990) 673-688.
[2] T.V. Duggan, J. Byrne, Factors Affecting Fatigue Behaviour, Fatigue as a Design Criterion, Springer1977, pp. 1-25.
[3] I. Nikulin, T. Sawaguchi, K. Tsuzaki, Effect of alloying composition on low-cycle fatigue properties and microstructure of Fe–30Mn–(6− x) Si–xAl TRIP/TWIP alloys, Materials Science and Engineering: A 587 (2013) 192-200.
[4] S. Nagarjuna, M. Srinivas, K. Balasubramanian, D. Sarmat, Effect of alloying content on high cycle fatigue behaviour of Cu-Ti alloys, International journal of fatigue 19(1) (1997) 51-57.
[5] F. Ostermann, Improved fatigue resistance of Al-Zn-Mg-Cu (7075) alloys through thermomechanical processing, Metallurgical and Materials Transactions B 2(10) (1971) 2897-2902.
[6] R. Boyer, H. Rack, V. Venkatesh, The influence of thermomechanical processing on the smooth fatigue properties of Ti–15V–3Cr–3Al–3Sn, Materials Science and Engineering: A 243(1) (1998) 97-102.
[7] R.W. Landgraf, R.A. Chernenkoff, Residual stress effects on fatigue of surface processed steels, Analytical and experimental methods for residual stress effects in fatigue, ASTM International1988.
[8] G. Webster, A. Ezeilo, Residual stress distributions and their influence on fatigue lifetimes, International Journal of Fatigue 23 (2001) 375-383.
[9] V. Levitin, S. Loskutov, The effect of a current pulse on the fatigue of titanium alloy, Solid state communications 131(3) (2004) 181-183.
[10] Y. Tang, A. Hosoi, Y. Morita, Y. Ju, Restoration of fatigue damage in stainless steel by high-density electric current, International Journal of Fatigue 56 (2013) 69-74.
[11] Y. Tang, A. Hosoi, Y. Iwase, Y. Ju, Effect of high-density electric current on the microstructure and fatigue crack initiation of stainless steel, Materials Transactions 54(11) (2013) 2085-2092.
[12] S. Konovalov, A. Atroshkina, Y.F. Ivanov, V. Gromov, Evolution of dislocation substructures in fatigue loaded and failed stainless steel with the intermediate electropulsing treatment, Materials Science and Engineering: A 527(12) (2010) 3040-3043.
[13] S. Konovalov, I. Komissarova, D. Kosinov, V. Gromov, A. Semin, Increase in Reliability of Metal Articles with Impulse Current Effect, MATEC Web of Conferences, EDP Sciences, 2016, p. 06109.

[14] Y. Zhao, Y. Liang, W. Zhou, Q. Qin, Q. Jiang, Effect of a current pulse on the thermal fatigue behavior of cast hot work die steel, ISIJ international 45(3) (2005) 410-412.
[15] O. Sosnin, A. Gromova, E.Y. Suchkova, E. Kozlov, Y.F. Ivanov, V. Gromov, The structural-phase state changes under the pulse current influence on the fatigue loaded steel, International Journal of Fatigue 27(10) (2005) 1221-1226.
[16] O. Sosnin, A. Gromova, Y.F. Ivanov, S. Konovalov, V. Gromov, E. Kozlov, Control of austenite steel fatigue strength, International Journal of Fatigue 27(10) (2005) 1186-1191.
[17] H. Lin, Y. Zhao, Z. Gao, L. Han, Effects of pulse current stimulation on the thermal fatigue crack propagation behavior of CHWD steel, Materials Science and Engineering: A 478(1) (2008) 93-100.
[18] A. Hosoi, T. Kishi, Y. Ju, Healing of fatigue crack by high-density electropulsing in austenitic stainless steel treated with the surface-activated pre-coating, Materials 6(9) (2013) 4213-4225.
[19] A. Hosoi, T. Yano, Y. Morita, Y. Ju, Quantitative evaluation of the displacement distribution and stress intensity factor of fatigue cracks healed by a controlled high-density electric current field, Fatigue & Fracture of Engineering Materials & Structures 37(9) (2014) 1025-1033.
[20] A. Hosoi, T. Nagahama, Y. Ju, Fatigue crack healing by a controlled high density electric current field, Materials Science and Engineering: A 533 (2012) 38-42.
[21] Y. Fahmy, T. Hare, R. Tooke, H. Conrad, Effects of a pulsed magnetic treatment on the fatigue of low carbon steel, Scripta materialia 38(9) (1998) 1355-1358.
[22] L. Bao-Tong, Q. Sheng-Ru, S. Xiao-Yan, Exploration on repairing fatigue damage of steel specimens with magnetic treatment, Scripta materialia 40(7) (1999) 767-771.
[23] A. Çelik, A.F. Yetim, A. Alsaran, M. Karakan, Effect of magnetic treatment on fatigue life of AISI 4140 steel, Materials & design 26(8) (2005) 700-704.
[24] G. Karpenko, O. Kuzin, V. Tkachev, V. Rudenko, Influence of an electric current upon the low-cycle fatigue of steel, Sov Phys Dokl, 1976, pp. 159-160.
[25] H. Conrad, J. White, W. Cao, X. Lu, A. Sprecher, Effect of electric current pulses on fatigue characteristics of polycrystalline copper, Materials Science and Engineering: A 145(1) (1991) 1-12.
[26] J. Jung, Y. Ju, Y. Morita, Y. Toku, Effect of pulsed electric current on the growth behavior of fatigue crack in Al alloy, Procedia Structural Integrity 2 (2016) 2989-2993.
[27] M. Mohin, H. Toofanny, A. Babutskyi, A. Lewis, Y. Xu, Effect of Electromagnetic Treatment on Fatigue Resistance of 2011 Aluminum Alloy, Journal of Multiscale Modelling 7(03) (2016) 1650004.
[28] G. Taguchi, S. Konishi, Taguchi Methods: Orthogonal Arrays and Linear Graphs-Tools for Quality Engineering, American Supplier Institute, Center for Taguchi Methods1987.
[29] M. Demirci, A. Samanchi, N. Tarakcioglu, T. Asilturk, optimization of fatigue life parameters with Taguchi Method, 6th International Advanced Technologies Symposium (IATS'11), 2011, pp. 16-18.
[30] K. Aluminium, Rod & bar alloy (2011 and 2014) technical data, Kaiser Aluminum, 2016, pp. 1-2.
[31] R. Wilson, Guide to the effect of shot peening on fatigue strength, Engineering Sciences Data Unit 1 (1992) 1-42.
[32] H.V. Chavan, M.S. Yadav, Investigate the effect of phosphate surface coating on the fatigue performance of the piston pin materials, Technology 6(11) (2015) 244-250.
[33] D.O. Macodiyo, H. Soyama, Optimization of cavitation peening parameters for fatigue performance of carburized steel using Taguchi methods, Journal of Materials Processing Technology 178(1) (2006) 234-240.
[34] C. Vidal, V. Infante, P. Vilaça, Assessment of improvement techniques effect on fatigue behaviour of friction stir welded aerospace aluminium alloys, Procedia Engineering 2(1) (2010) 1605-1616.
[35] M. Minitab 17.0, LLC,, A commertially available statistical software, 2014. https://www.minitab.com/en-us/.
[36] C. Xie, S. Yang, H. Liu, Q. Zhang, Y. Wang, Y. Zou, Microstructure and mechanical properties of robot cold metal transfer Al5. 5Zn2. 5Mg2. 2Cu aluminium alloy joints, Journal of Materials Processing Technology 255 (2018) 507-515.
[37] E. Dudrová, M. Kabátová, Fractography of sintered iron and steels, Powder Metallurgy Progress 8(2) (2008) 59-75.
[38] M. Moeser, Fractography with the SEM (failure analysis), 2007.
[39] J. Zhou, S. Xu, S. Huang, X. Meng, J. Sheng, H. Zhang, J. Li, Y. Sun, E.A. Boateng, Tensile Properties and Microstructures of a 2024-T351 Aluminum Alloy Subjected to Cryogenic Treatment, Metals 6(11) (2016) 279.

[40] G.-R. Li, J.-F. Cheng, H.-M. Wang, P.-S. Li, C.-Q. Li, Influence of a high pulsed magnetic field on the tensile properties and phase transition of 7055 aluminum alloy, Materials Research Express 3(10) (2016) 106507.
[41] G. Zhang, J. Zhang, B. Li, W. Cai, Double-stage hardening behavior and fracture characteristics of a heavily alloyed Al–Si piston alloy during low-cycle fatigue loading, Materials Science and Engineering: A 561 (2013) 26-33.
[42] H.A. Wheeler, Formulas for the skin effect, Proceedings of the IRE 30(9) (1942) 412-424.
[43] C. Yang, W. Xu, B. Guo, D. Shan, J. Zhang, Healing of fatigue crack in 1045 steel by using eddy current treatment, Materials 9(8) (2016) 641.
[44] H. Conrad, Electroplasticity in metals and ceramics, Materials Science and Engineering: A 287(2) (2000) 276-287.
[45] H. Conrad, Thermally activated plastic flow of metals and ceramics with an electric field or current, Materials Science and Engineering: A 322(1-2) (2002) 100-107.
[46] R.W. Christy, A. Pytte, The structure of matter: an introduction to modern physics, WA Benjamin1965.
[47] A. Babutskyi, A. Chrysanthou, M. Smelina, G. Stepanov, M. Ziętara, Effect of pulsed magnetic treatment on the corrosion of titanium, Materials Science and Technology (2017) 1-12.
[48] S. Wu, H. Zhao, A. Lu, H. Fang, F. Tang, A micro-mechanism model of residual stress reduction by low frequency alternating magnetic field treatment, Journal of materials processing technology 132(1) (2003) 198-202.
[49] L. Ma, W. Zhao, Z. Liang, X. Wang, L. Xie, L. Jiao, T. Zhou, An investigation on the mechanical property changing mechanism of high speed steel by pulsed magnetic treatment, Materials Science and Engineering: A 609 (2014) 16-25.
[50] M. Molotskii, Possible mechanism of the magnetoplastic effect, Soviet physics. Solid state 33(10) (1991) 1760-1761.
[51] M. Molotskii, Negative magnetoplastic effect in nonmagnetic crystals, Physics of the solid state 35 (1993) 5-7.
[52] M. Molotskii, V. Fleurov, Spin effects in plasticity, Physical review letters 78(14) (1997) 2779.
[53] M.I. Molotskii, Theoretical basis for electro-and magnetoplasticity, Materials Science and Engineering: A 287(2) (2000) 248-258.
[54] G. Ravichandran, A.J. Rosakis, J. Hodowany, P. Rosakis, On the conversion of plastic work into heat during high-strain-rate deformation, AIP conference proceedings, AIP, 2002, pp. 557-562.
[55] T.R. Prabhu, Effects of ageing time on the mechanical and conductivity properties for various round bar diameters of AA 2219 Al alloy, Engineering Science and Technology, an International Journal 20(1) (2017) 133-142.
[56] Z. Pakiela, K. Ludwichowska, J. Ferenc, M. Kulczyk, Mechanical properties and electrical conductivity of Al 6101 and 6201 alloys processed by hydro-extrusion, IOP Conference Series: Materials Science and Engineering, IOP Publishing, 2014, p. 012120.
[57] M.A. Salazar-Guapuriche, Y. Zhao, A. Pitman, A. Greene, Correlation of strength with hardness and electrical conductivity for aluminium alloy 7010, Materials science forum, Trans Tech Publ, 2006, pp. 853-858.
[58] I. Polmear, Light alloys: from traditional alloys to nanocrystals, Elsevier2005.
[59] J.I. Jang, Estimation of residual stress by instrumented indentation: A review, J. Ceram. Process. Res 10(391) (2009) 1996-1944.
[60] S. Akram, A. Babutskyi, A. Chrysanthou, D. Montalvão, N. Pizurova, Effect of Alternating Magnetic Field on the Fatigue Behaviour of EN8 Steel and 2014-T6 Aluminium Alloy, Metals 9(9) (2019) 984.